Load Aggregation Effect in Power Grid

L. Shalalfeh[1] and E. Jonckheere[1]

***Abstract*— In this paper, the issue of data-driven modeling of a single load in a laboratory set-up is confronted with the same data-driven modeling of the same load, but in a real grid environment. As it is argued here, an aggregation effect of all of the loads in a grid endows a single load with grid-characteristics properties in addition to the usual load-specific properties. Topologically, the hidden feedback structure of a bus model reveals that the resulting digraph is strongly connected, meaning that all loads are intertwined in a single system that cannot be decomposed into islands.**

I. Introduction

Load modeling is undoubtedly an important—still active—area of research in the power grid. Indeed, depending on their active and reactive power profiles, loads could be the culprit in voltage collapse or other nuisances in the grid [8], [24]. One issue that has never been made completely clear is what is the difference between, on the one hand, a model of a single isolated load and, on the other hand, a model of a load in a complex grid environment. Berg [4], [5] is adamant that his load models represent the loads in the Scandinavian microgrid environment in which the experiments were done. Hill [14], [20] on the other hand does "curve fitting" of the power disruption resulting from a voltage drop in a single load laboratory environment. A puzzling difference between the two models is that the Berg model involves the frequency in a fractional exponent in a narrow bandwidth around 50 cycles/sec, whereas a lingering issue in the Hill model is its lack of frequency dependence [14, p. 175], [21, p. 24].

A fractional transfer function model of a high voltage transformer was already derived in [15]. The big difference is that the fractional model of the transformer is mandated by matching the frequency response *over a very large frequency sweep,* exciting parasitic distributed parameter electromagnetic effects present in the wiring of the transformer. Here, we deal with the frequency response *over a very narrow frequency band around 50 cycles/sec.* Under those circumstances, it is a bit difficult to see how parasitic modes could be excited, unless another hitherto unknown effect is present. The purpose of this paper is to offer evidence that his other effect is the aggregation of the loads. By "load aggregation," we mean that, after unraveling the hidden feedbacks in bus model, the resulting interconnected system is made up of one and only one strongly connected component [6], [7]. The latter means that under normal operations loads are not "islanded." Quite to the contrary, *every single load penetrates the whole grid.* As an example [12], removing a load at a grid point in the Bay Area was observed by a micro-PMU 550 kilometers away in the Los Angeles area.

An outline of the paper follows: Sec. II deals with Berg load modeling. Sec. III introduces the basic feedback motif of a single generator, single line, single load bus. This basic feedback motif is repeated to reveal the hidden feedback structure of a more complicated grid in Sec. IV. Sec. V describes the load aggregation effect as the strongly connected property of the hidden feedback structure. Sec. VI describes various contingency scenarios.

II. Berg Load modeling and fractional dynamics

The Berg model [1], [4], [5],

$$P(V_L,\omega)=K_pV_L^{p_v}\omega^{p_\omega},\quad Q(V_L,\omega)=K_qV_L^{q_v}\omega^{q_\omega},\quad (1)$$

is usually thought of as a static model, but its frequency dependence gives it some dynamical properties formalized in the describing function technique [2]. The Berg model was derived experimentally from data collected on a Scandinavian "micro-grid," when a generator was deliberately removed from the grid, resulting in transients and eventually a new steady state of the power profile (P,Q) absorbed by the load. Contrary to the Hill model, the Berg model does not attempt to model the transients; it only models the shift in the steady state, but in a manner that goes beyond the Hill model as it involves the frequency—in a rather unorthodox way, with fractional exponents of the frequency.

It is straightforward to go from the complex power to the impedance model of the load:

$$\mathbf{Z_L}=\frac{\mathbf{V_L}\mathbf{V_L}^*}{\mathbf{I_L}\mathbf{V_L}^*}=\frac{V_L^2}{\mathbf{S_L}^*}=\frac{V_L^2}{P(V_L,\omega)-jQ(V_L,\omega)}=\frac{1}{K_pV_L^{p_v-2}\omega^{p_\omega}-jK_qV_L^{q_v-2}\omega^{q_\omega}},\quad (2)$$

where boldfaced quantities denote phasors and where $\mathbf{S_L}=\mathbf{V_L}\mathbf{I_L}^*=P(V_L,\omega)+jQ(V_L,\omega)$ is the complex power. Using the experimental p_v, p_ω, q_v, and q_ω data derived in [4] for different loads, the impedances are easily obtained as in [24, Table II], in describing function format [2] since they depend on the voltage amplitude.

For notational convenience, we switch to the admittance formulation $\mathbf{Y}_L=1/\mathbf{Z}_L=L\omega^p-jW\omega^q$. Next, we approximate $\mathbf{Y}_L(V_L,\omega)$ with a formal circuit-theoretic admittance, except for its amplitude dependency,

$$\mathbf{Y}_L(V_L,\omega)\approx A(V_L)\times(j\omega)^\alpha-B(V_L)\times(j\omega)^\beta,\quad (3)$$

where A, B are real-valued. The construction of the approximation is done as follows: First, write $j^\alpha=a+jb, j^\beta=$

(1) Dept. of Electrical Engineering, Univ. of Southern California, Los Angeles, CA 90089-2563 {shalalfe,jonckhee}@usc.edu

$c + jd$. Then the approximant becomes

$$A\times(j\omega)^\alpha - B\times(j\omega)^\beta = aA\omega^\alpha - cB\omega^\beta + j(bA\omega^\alpha - dB\omega^\beta).$$

The matching conditions then become

$$aA\omega^\alpha - cB\omega^\beta \approx L\omega^p, \quad -bA\omega^\alpha + dB\omega^\beta \approx W\omega^q.$$

Matching the right and left-hand sides at $\omega = \omega_0 = 2\pi 50$ rad/sec, along with the derivatives around $\omega = \omega_0$, entails 4 conditions. This allows us to uniquely determine the 4 parameters A, α, B, β.

The right-hand side of (3) has an obvious holomorphic extension, $A\times(\sigma+j\omega)^\alpha - B\times(\sigma+j\omega)^\beta$ that clearly satisfies the Cauchy-Riemann conditions. For $\omega = 0$, the extension is obviously real and hence satisfies the "realness" condition of formal circuit theory [3].

Finally, write $s = \sigma + j\omega$, the Laplace symbol. With this notation, the admittance takes the form

$$\mathbf{Y}_L = \frac{\mathbf{I}_L}{\mathbf{V}_L} = As^\alpha - Bs^\beta.$$

Reinterpreting the inverse Laplace transform of s^α as the fractional differential $D^\alpha_{(*)}$ yields the fractional dynamics model:

$$I_L(t) = AD^\alpha_* V_L(t) - BD^\beta_* V_L(t). \tag{4}$$

In our choice between the Riemann D^α and the Caputo D^α_* fractional differential [11], [13], [16], [17], [18], [19], we opted for the latter as its initial conditions involves only integer order derivatives of V_L. Note that such a fractional order equation is known not to have periodic solutions [25]. It is believed that the fluctuations of the PMU variables observed in [22] betray their fractional dynamics.

III. Basic motif

In the most basic power system (one generator with internal impedance, one line, one load), a feedback structure already appears in the light of its circuit theoretic model. The basic bus model of Fig. 1(a) has the 2-motif feedback structure of Fig. 1(b). The first motif refers to the loop $Z_G Y_{12}$ fed by the generator emf E_G to produce the generator voltage V_G, as shown in the top part of Fig. 1(b). The second motif is the $Z_L Y_{12}$ loop that produces the load voltage V_L. In the next section, we analyze those two basic motifs are repeated in a large scale architecture to yield the hidden feedback structure in the power grid.

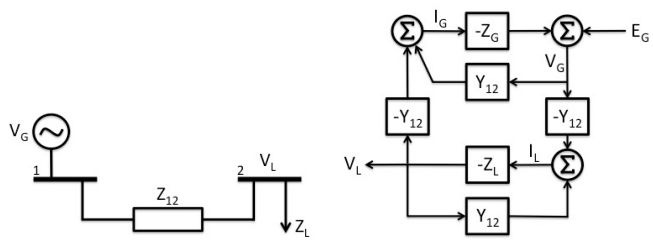

(a) (b)

Fig. 1: Simple 2-bus power system: (a) Circuit diagram (b) Feedback model

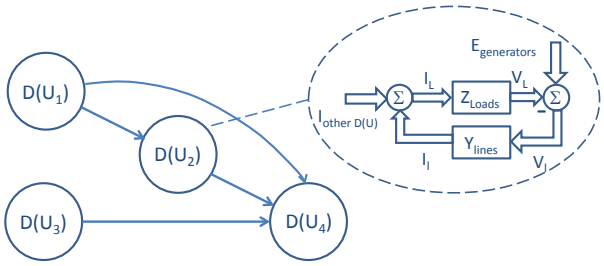

Fig. 2: Hypothetical decomposition of a grid digraph into strongly connected components. Each strongly connected component (dotted circle) is itself a multivariable version of the bottom motif of Fig. 1(b).

IV. Basic motif interconnection

Consider now the basic motif of Fig. 1(a) repeated in an interconnection pattern together with the basic feedback of Fig. 1(b) itself repeated in a matter consistent with the bus model. The latter obviously leads to a complicated feedback interconnect.

Given a complicated feedforward-feedback path interconnection, the question as to whether closed-loop stability could be decided by examining closed-loop stability of several "subsystems" was posed in a graph-theoretic setting by Callier and Desoer [6], [7]. Given that transport of the various information/commodities occurs in a specific direction, the overall interconnection structure can be abstracted as a *directed graph* or *digraph* $\mathcal{D} = (\mathcal{V}, \mathcal{E})$. A *Strongly Connected Component (SCC),* $\mathcal{D}(U)$, $U \subseteq \mathcal{V}$, is a subset of vertices and oriented edges connecting U-vertices such that $\forall v_i, v_j \in \mathcal{D}(U)$, there exists a directed path from v_i to v_j and a directed path from v_j to v_i, and furthermore the subset is maximal in the sense that adding a vertex $v_k \notin U$ would destroy the strongly connected property. The SCCs are themselves connected through the Interconnection Subsystem (IS), which, as shown in Fig. 2, has no oriented loops for otherwise some of the $\mathcal{D}(U_i)$ could not be maximal. Then using the concept of essential set, each SCC component is partitioned into two parts: one that is the feedforward path and another that is the feedback part of the diagram, as illustrated in the dotted circle of Fig. 2.

We apply those concepts of [6], [7] to the power grid. Instead of arguing in terms of active/reactive power flow, we argue in terms of such circuit theory commodities as generator electro-motive forces (E_G), line voltage drops (V_ℓ), line currents (I_ℓ), load voltages (V_L), and load currents (I_L). It is argued that the circuit theory interconnection has a great many feedbacks, hidden in the bus model, but revealed upon modeling the loads as impedances. Indeed, repeating the bottom motif of Fig. 1(b) yields the multivariable feedback shown in the dotted circle of Fig. 2, where the load impedances are in the feedforward path and the line admittances in the feedback path, although the reverse convention shown in the bottom motif Fig. 1(b) is fundamentally not different.

Looking at the hypothetical decomposition of Fig. 2, it follows that, if a collapse occurs in one of the $\mathcal{D}(U_i)$'s, that part of the network upstream to $\mathcal{D}(U_i)$ won't be affected. Now, assume there is adequate supply relative to the demand. Assume none of the $\mathcal{D}(U_i)$'s could go into the nonlinear feedback effect collapse as formulated in [24]. Then the whole interconnect would not go into collapse. Clearly, if such a decomposition as that of Fig. 2 were possible, checking for collapse would be immensely simplified and two loads in different $\mathcal{D}(U_i)$'s won't be aggregated in a feedback loop.

The problem is that for any grid with the generator internal impedances properly modeled, except in case of faults, the hidden feedback structure is strongly connected, cannot be decomposed in strongly connected component, and the various loads are intertwined in an aggregating feedback.

V. Aggregation effect: one single Strongly connected component

Before going through the detail, we provide an idea of the proof of Th. 1. Consider a 1-generator, 2-load interconnect, as shown in Fig. 3. Going from power flow to equivalent circuit theoretical formulation yields the multi-input, multi-output (MIMO) feedback of Fig. 4(a). By visual inspection, the latter interconnect looks like the MIMO feedback shown in the dotted circle of Fig. 2, with the extra difficulty that Fig. 4(a) involves generator internal impedance. The nodes of the feedback diagram of Fig. 4(a) are partitioned into voltage nodes and current nodes in the bipartite digraph shown in Fig. 4(b), obviously strongly connected. From this point on, it turns out that adding one generator will add another bipartite digraph, the two digraphs being connected in a way that allows us to go back and forth between the two of them. It turns out that this is a general fact; hence the hidden feedback graph is strongly connected.

1) 3-bus power system: In this case, we choose a 3-bus system with one generator at bus 2 feeding two loads at buses 1 and 3, as shown in Fig. 3. The feedback structure of this power system, depicted in Fig. 4(a), has three motifs, one for the generator and two for the loads. By looking at the feedback system, we can see that the generator is connected to the loads Z_{L1} and Z_{L2} through line admittances Y_{12} and Y_{23} respectively. So, the system is strongly connected.

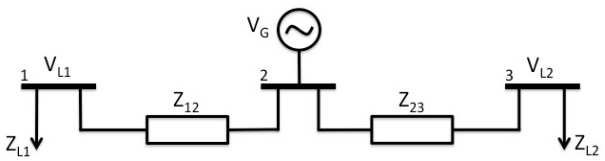

Fig. 3: 3-bus power system: 1 generator, 2 loads

The graph of this feedback system is a bipartite 2-color graph, as shown in Fig. 4(b). The green color is for the voltage nodes (V_{L1}, V_G, and V_{L2}) and the orange color is for the current nodes (I_{L1}, I_G, and I_{L2}).

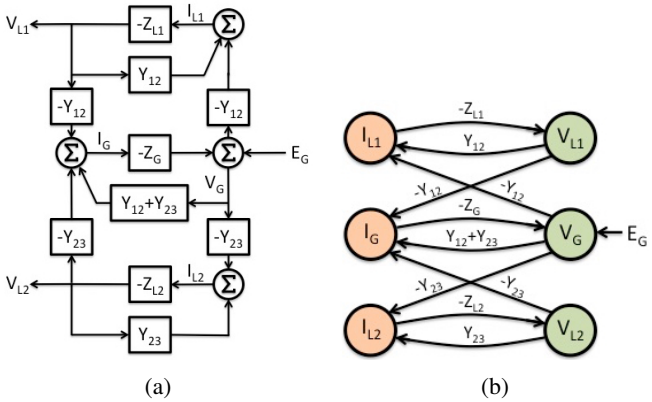

Fig. 4: 3-motif case (1 generator, 2 loads): (a) Feedback model, (b) Graph model

We can find the "plant" transfer matrix $\bar{G}$ and the feedback matrix $\bar{F}$ by writing the nodal equations for the power system, which yields

$$\underbrace{\begin{bmatrix} V_{L1} \\ V_G \\ V_{L2} \end{bmatrix}}_{\eta} = \underbrace{\begin{bmatrix} -Z_{L1} & 0 & 0 \\ 0 & -Z_G & 0 \\ 0 & 0 & -Z_{L2} \end{bmatrix}}_{\bar{G}} \underbrace{\begin{bmatrix} I_{L1} \\ I_G \\ I_{L2} \end{bmatrix}}_{e} + \underbrace{\begin{bmatrix} 0 \\ E_G \\ 0 \end{bmatrix}}_{V}, \quad (5)$$

$$\underbrace{\begin{bmatrix} I_{L1} \\ I_G \\ I_{L2} \end{bmatrix}}_{e} = \underbrace{\begin{bmatrix} Y_{12} & -Y_{12} & 0 \\ -Y_{12} & Y_{12}+Y_{23} & -Y_{23} \\ 0 & -Y_{23} & Y_{23} \end{bmatrix}}_{\bar{F}} \underbrace{\begin{bmatrix} V_{L1} \\ V_G \\ V_{L2} \end{bmatrix}}_{\eta}. \quad (6)$$

2) 6-bus power system: In this case, we have a larger power system with 6 buses, 2 generators, and 4 loads as shown in Fig. 5 . The feedback model of the power system, as shown in Fig. 6(a), has 6 motifs, two for the generators and four for the loads 1, 2, 3, and 4. The feedback model is strongly connected.

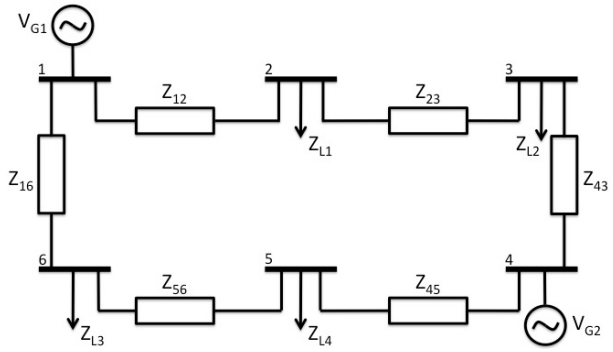

Fig. 5: 6-bus power system

The graph representation of this power system, depicted in Fig. 6, shows how generator and load motifs are connected. The graph is strongly connected, because the only way of decomposing the graph is by disconnecting two lines in the system, like lines 2-3 and 5-6.

The plant matrix $\bar{G}$ and the feedback matrix $\bar{F}$ are derived below

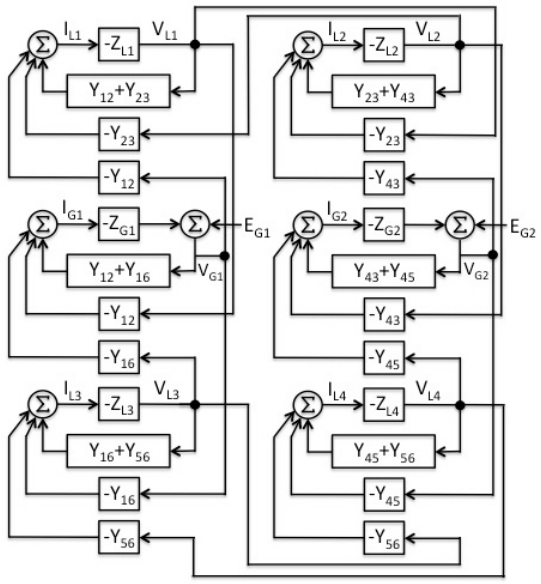

(a)

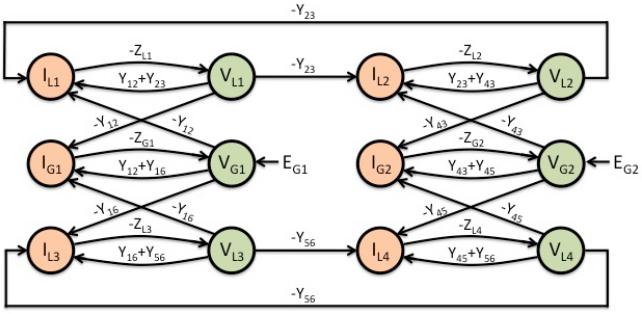

(b)

Fig. 6: 6-motif case: (a) Feedback model, (b) Graph model

$$\underbrace{\begin{bmatrix} V_{G1} \\ V_{L1} \\ V_{L2} \\ V_{G2} \\ V_{L4} \\ V_{L3} \end{bmatrix}}_{\eta} = \bar{G} \underbrace{\begin{bmatrix} I_{G1} \\ I_{L1} \\ I_{L2} \\ I_{G2} \\ I_{L4} \\ I_{L3} \end{bmatrix}}_{e} + \underbrace{\begin{bmatrix} E_{G1} \\ 0 \\ 0 \\ E_{G2} \\ 0 \\ 0 \end{bmatrix}}_{V},$$

$$\bar{G} = \begin{bmatrix} -Z_{G1} & 0 & 0 & 0 & 0 & 0 \\ 0 & -Z_{L1} & 0 & 0 & 0 & 0 \\ 0 & 0 & -Z_{L2} & 0 & 0 & 0 \\ 0 & 0 & 0 & -Z_{G2} & 0 & 0 \\ 0 & 0 & 0 & 0 & -Z_{L4} & 0 \\ 0 & 0 & 0 & 0 & 0 & -Z_{L3} \end{bmatrix};$$

$$\underbrace{\begin{bmatrix} I_{G1} \\ I_{L1} \\ I_{L2} \\ I_{G2} \\ I_{L4} \\ I_{L3} \end{bmatrix}}_{e} = \bar{F} \underbrace{\begin{bmatrix} V_{G1} \\ V_{L1} \\ V_{L2} \\ V_{G2} \\ V_{L4} \\ V_{L3} \end{bmatrix}}_{\eta},$$

$$\bar{F} = \begin{bmatrix} Y_{12}+Y_{16} & -Y_{12} & 0 & 0 & 0 & -Y_{16} \\ -Y_{12} & Y_{12}+Y_{23} & -Y_{23} & 0 & 0 & 0 \\ 0 & -Y_{23} & Y_{23}+Y_{43} & -Y_{43} & 0 & 0 \\ 0 & 0 & -Y_{43} & Y_{43}+Y_{45} & -Y_{45} & 0 \\ 0 & 0 & 0 & -Y_{45} & Y_{45}+Y_{56} & -Y_{56} \\ -Y_{16} & 0 & 0 & 0 & -Y_{56} & Y_{16}+Y_{56} \end{bmatrix}$$

3) IEEE 14-bus power system: This 14-bus power system is one of the IEEE standard test cases which was provided online by [10] and depicted in Fig. 7 with its graph model shown in Fig. 8.

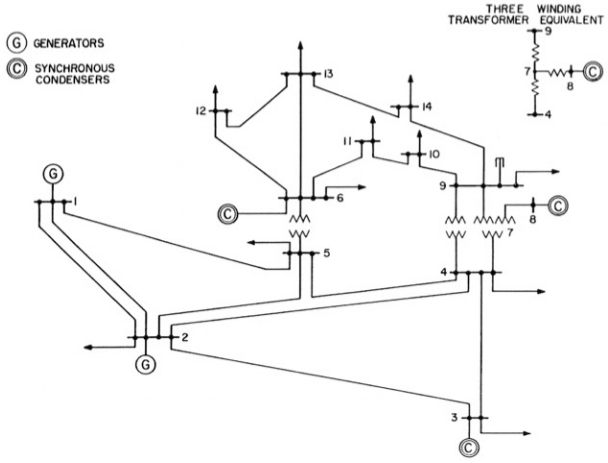

Fig. 7: IEEE 14 bus power system

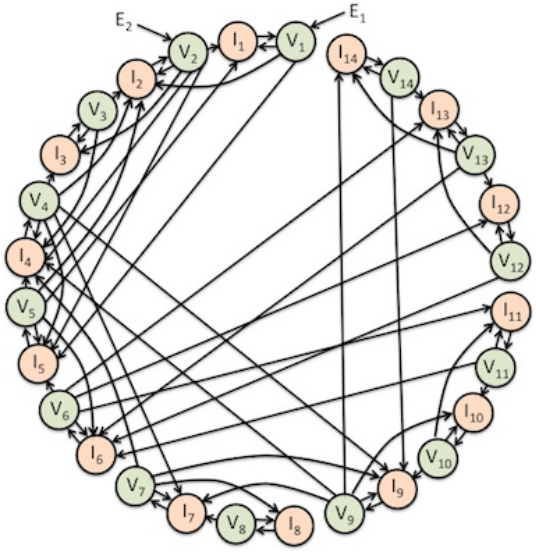

Fig. 8: Graph model in Small World configuration

In view of the above many examples, we can formulate the following major result of the paper:

Theorem 1: Under the condition that the bus system has no faults, if the bus model graph is connected, then it is strongly connected.

Proof: The grid is composed of many "basic motifs," each motif being strongly connected. Given two motifs, say i and j, since the graph is connected, there are intermediate motifs, $i+1$, $i+2$, ..., $j-2$, $j-1$, connected with directed

edges $\{i, i+1\}$, $\{i+1, i+2\}$,..., $\{j-1, j\}$, where $\{k, k+1\}$ denotes an edge without specification of its direction. Physically, each edge $\{k, k+1\}$ is an admittance Y flowing in one direction. But by the feedback created by this line admittance, there is another edge Y flowing in the other direction. Hence two consecutive motifs, say, k and $k+1$ are connected by two edges: one $k \to k+1$ and another one $k+1 \to k$. Hence the graph is strongly connected. ■

VI. The effect of contingencies on the power system graph

In Section V, we were able to show that any power system has a strongly connected feedback digraph. In this section, we show how the power system digraph can lose its strong connectivity in case of single-element $(N-1)$ and double-element $(N-2)$ contingencies.

There are different types of contingencies in the power system like, generator failure, transformer failure, transmission line disconnection, faults (single phase to ground, phase-to-phase, three-phase). Here, we will consider only transmission line tripping and three-phase fault and we will choose the 6-bus power system as our case study.

A. Single-element contingency

In the graph shown in Fig. 6(b), each transmission line connects the two bipartite graphs by two edges in both directions. Disconnecting any transmission line randomly will not effect the strong connectivity of the graph. For example, if the line 5-6 is disconnected, the edges V_{L3}-I_{L4} and V_{L4}-I_{L3} will disappear from the graph, but the remaining 2-3 line will ensure strong connectivity of the 2 bipartite graph interconnect. The weight of the edges connecting V_{L3}-I_{L3} and V_{L4}-I_{L4} will become Y_{16} and Y_{45}, respectively.

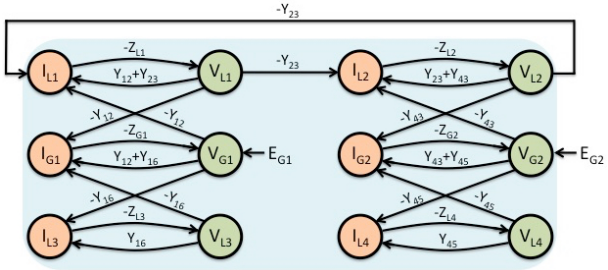

Fig. 9: Graph model of 6-bus power system after disconnecting line 5-6

In case of a three-phase fault, the load impedance and the voltage at bus load become zero. Since the voltage at the load bus is zero, we can delete its vertex and all the edges connected to it. A fault at any of the loads will make the graph not strongly connected any more because there is no edge leaving the current vertex at the faulted bus. So, the graph will have two strongly connected components, one for the load current and the other one for the remaining vertices. For example, a three-phase fault at load 1 has a graph as the one shown in Fig.10.

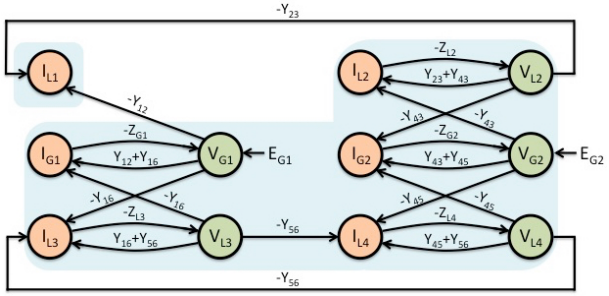

Fig. 10: Graph model of 6-bus power system after a three-phase fault at bus 2

B. Double-element contingency

Disconnecting any two transmission lines from the power system will cause removing four edges from the graph, 2 for each line. This kind of contingencies can make the system not strongly connected anymore and divide the graph into two smaller strongly connected ones. This kind of contingencies is very harmful to the power system, especially when the generation does not meet the demand in the new separated parts.

If we disconnect the lines 2-3 and 5-6, the new graph will have 2 strongly connected components, each component with 1 generator and 2 loads, as shown in Fig.11.

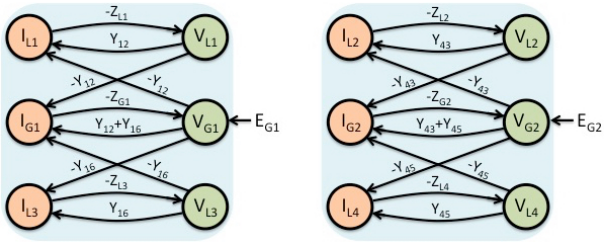

Fig. 11: Graph model of 6-bus power system after disconnecting lines 2-3 and 5-6

In case of two three-phase faults, all the edges connected to the two voltage vertices will disappear as well as the two vertices themselves. The effect caused by these faults will be four strongly connected components, two of them have only one vertex and the other two have four vertices. If we choose for example load 1 and load 4 to have faults, the resulted graph model is shown in Fig.12.

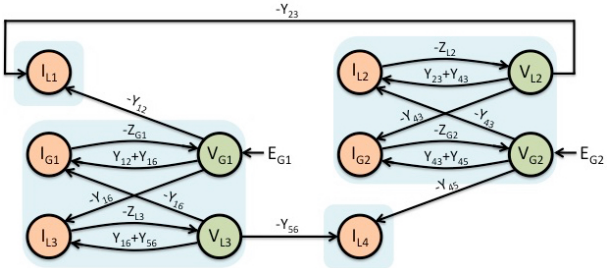

Fig. 12: Graph model of 6-bus power system after faults at buses 2 and 5

The connected but not strongly connected cases of Figs. 10, 12 illustrate the necessity to restrict Theorem 1 to systems that have no faults.

VII. Conclusion

A. Summary

The main point of the paper is encapsulated in Theorem 1, saying that the hidden feedback structure of the power grid—essential for understanding subtle voltage collapse scenarios [24]—is strongly connected [6], [7]. The latter is a robust property, as it survives some simple contingencies as shown in Sec. VI. This strongly connected property means that the great many loads in the power grid are intertwined, so that (P, Q) measurements made at one load do not reflect the nominal load behavior, but its behavior in the grid environment. At the limit of infinitely many loads, the nominal load will appear to have a distributed parameter frequency response, as the Berg model (1) shows.

Parallel to this "first principles" approach, the fractal analysis of PMU signals [22], [23] points to the necessity of the Grünwald-Letnikov fractional dynamics [9] to explain the behavior of the signals. On the other hand, after some holomorphic extension of the Berg model, the inverse Laplace transform yields a Riemann-Caputo fractional dynamics [13], hence connecting the data driven and first principles approaches.

Another corollary of the strongly connected component is that cascading failures are unlikely to be contained without human intervention.

B. Future work

The Berg model [4] somehow misses the transient that leads to the perturbed steady state after voltage disruption, which is precisely taken care of by the Hill model [14]. Incorporating the Hill modeling of the transients in the Berg model would lead to the next generation of load models.

Establishing the complete connection between the fractal PMU data-driven analysis and the first principles approach, relying on the Grünwald-Letnikov and the Riemann-Caputo fractional derivatives, respectively, calls for some reconciliation between the two fractional dynamics approaches.

References

[1] J. Arrillaga and C. P. Arnold. *Computer Analysis of Power Systems*. John Wiley and Sons, Chichester, New York, Brisbane, Toronto, Singapore, 1990.

[2] D. P. Atherton. *Stability of Nonlinear Systems*. Research Studies Press, New York, 1981.

[3] V. Belevitch. *Classical Network Theory*. Holden-Day, San Francisco, 1968.

[4] G. J. Berg. System and load behavior following loss of generation—experimental results and evaluation. *Proc. IEE*, 119(10):1483–1486, October 1972.

[5] G. J. Berg. Power system load representation. *Proc. IEE*, 120(3):344–348, March 1973.

[6] F. M. Callier, W. S. Chan, and C. A. Desoer. Input-output stability theory of interconnected systems using decomposition techniques. *IEEE Transactions on Circuits and Systems*, CAS-23(12):714–729, December 1976.

[7] F. M. Callier, W. S. Chan, and C. A. Desoer. Input-output stability of interconnected systems using decompositions: An improved formulation. *IEEE Transactions on Automatic Control*, AC-23(2):150–163, April 1978.

[8] Claudio A. Canizares. On bifurcation, voltage collapse and load modeling. *IEEE Transactions on Power Systems*, 10(1):512–522, 1995.

[9] M. Chakraborty, D. Maiti, A. Konar, and R. Janarthanan. A study of the Grunwald-Letnikov definition for minimizing the effects of random noise on fractional order differential equations. In *Information and Automation for Sustainability, 2008. ICIAFS 2008. 4th International Conference on*, pages 449–456, Dec 2008.

[10] R. Christie. Uw power system test case archive. Available: http://www.ee.washington.edu/research/pstca/.

[11] F. Cipriano, H. Ouerdiane, and R. Vilela Mendes. Stochastic solution of a KPP-type nonlinear fractional differential equation. *Fractional Calculus and Applied Analysis*, 12(1):47–56, 2009.

[12] P. Fairley. Sniffing out grid attacks. *IEEE Spectrum*, pages 13–15, Sept. 2016.

[13] F. Gorenflo and F. Mainardi. Fractional calculus: Integral and differential equations of fractional order. In A. Carpinteri and F. Mainardi, editors, *Fractals and Fractional Calculus in Continuum Mechanics*, pages 223–276. Springer, New York, 1997.

[14] D. J. Hill. Nonlinear dynamic load models with recovery for voltage stability studies. *IEEE Transactions on Power Systems*, 8(1):166–176, February 1993.

[15] A . K. Kamath, J. R. Gandhi, A. S. Bohra, A. V. Goel, D. U. Patil, O. V. Kulkarni, and J. O. Chandle. Modeling of transformer characterisitics using fractional order transfer functions. In *IEEE International Conference on Control and Automation*, pages 2123–2128, Christchurch, New Zealand, December 2009.

[16] F. Mainardi, Y. Luchko, and G. Pagnini. The fundamental solution of the space-time fractional diffusion equation. *Fractional Calculus and Applied Analysis*, 4:153–192, 2001.

[17] R. Vilela Mendes and L. Vazquez. The dynamical nature of a backlash system with and without fluid friction. *Nonlinear Dynamics*, 47:363–366, 2007.

[18] V. Pipiras and M. S. Taqqu. Fractional calculus and its connections to fractional brownian motion. In P. Doukhan, G. Oppenheim, and M. S. Taqqu, editors, *Theory and Applications of Long-Range Dependence*, pages 165–201. Birkhuser, Boston, 2003.

[19] I. Podlubny. Geometric and physical interpretation of fractional integration and fractional differentiation. *Fractional Calculus and Applied Analysis*, 5:367–386, 2002.

[20] D. Popović, I. A. Hiskens, and D. J. Hill. Investigation of load-tap changer interaction. *Electrical Power & Energy Systems*, 18(2):81–97, 1996.

[21] M. Schwalbe. *Mathematical Science Research Challenges for the Next-Generation Electric Grid: Summary of a Workshop*. The National Academies Press, Washington, DC, 2015.

[22] L. Shalalfeh, P. Bogdan, and E. Jonckheere. Evidence of long range-dependence in power grid. In *Power and Energy Society General Meeting (PESGM)*, Boston, MA, July 2016. Available at `http://eudoxus2.usc.edu`.

[23] L. Shalalfeh, P. Bogdan, and E. Jonckheere. Kendall's tau of frequency Hurst exponent as blackout proximity margin. In *IEEE International Conference on Smart Grid Communications*, Sydney, Australia, 2016. To appear; available at `http:eudoxus2.usc.edu`.

[24] L. Shalalfeh and E. Jonckheere. The existence of a voltage collapse solution in the static-dynamic gap. In *American Control Conference (ACC)*, pages 4126–4131, Boston, MA, July 2016.

[25] M. S. Tavazoei and M. Haeri. A proof for non existence of periodic solutions in time invariant fractional order systems. *Automatica*, 46:1886–1890, 2009.